

Arbitrarily-Conditioned Multi-Functional Diffusion for Multi-Physics Emulation

Da Long

*Kahlert School of Computing
University of Utah*

U1368737@UTAH.EDU

Zhitong Xu

*Kahlert School of Computing
University of Utah*

U1502956@UTAH.EDU

Guang Yang

*Kahlert School of Computing
University of Utah*

U1326446@UTAH.EDU

Akil Narayan

*Kahlert School of Computing
University of Utah*

AKIL@SCI.UTAH.EDU

Shandian Zhe

*Kahlert School of Computing
University of Utah*

ZHE@CS.UTAH.EDU

Abstract

Modern physics simulation often involves multiple functions of interests, and traditional numerical approaches are known to be complex and computationally costly. While machine learning-based surrogate models can offer significant cost reductions, most focus on a single task, such as forward prediction, and typically lack uncertainty quantification — an essential component in many applications. To overcome these limitations, we propose Arbitrarily-Conditioned Multi-Functional Diffusion (ACM-FD), a versatile probabilistic surrogate model for multi-physics emulation. ACM-FD can perform a wide range of tasks within a single framework, including forward prediction, various inverse problems, and simulating data for entire systems or subsets of quantities conditioned on others. Specifically, we extend the standard Denoising Diffusion Probabilistic Model (DDPM) for multi-functional generation by modeling noise as Gaussian processes (GP). We then introduce an innovative denoising loss. The training involves randomly sampling the conditioned part and fitting the corresponding predicted noise to zero, enabling ACM-FD to flexibly generate function values conditioned on any other functions or quantities. To enable efficient training and sampling, and to flexibly handle irregularly sampled data, we use GPs to interpolate function samples onto a grid, inducing a Kronecker product structure for efficient computation. We demonstrate the advantages of ACM-FD across several fundamental multi-physics systems.

1. INTRODUCTION

Physical simulation plays a crucial role in numerous scientific and engineering applications. Traditional numerical approaches (Zienkiewicz et al., 1977; Mitchell and Griffiths, 1980), while offering strong theoretical guarantees, are often complex to implement and computationally expensive to run. In contrast, machine learning-based surrogate models (Kennedy and O’Hagan, 2000; Razavi et al., 2012), also known as emulators, trained on simulation or measurement data, can significantly reduce computational costs, making them a promising alternative.

However, modern physical simulations often involve multiple functions of interest, such as initial and boundary conditions, solution or state functions, parameter functions, source functions, and more. Current

machine learning-based surrogate models, such as neural operators (Li et al., 2020a; Lu et al., 2021; Kovachki et al., 2023), primarily focus on a single prediction task, for instance, forward prediction of the solution function. To perform other tasks, one typically needs to retrain a surrogate model from scratch. In addition, most existing models lack uncertainty quantification, which is important in many applications. For example, confidence intervals are important to assess the reliability of emulation results, and in inverse problems, a posterior distribution is required since such problems are often ill-posed.

To address these limitations, we propose Arbitrarily-Conditioned Multi-Functional Diffusion (ACM-FD), a versatile probabilistic surrogate model for multi-physics emulation. Within a single framework, ACM-FD can handle a wide range of tasks, including forward prediction with different input functions, various inverse problems conditioned on different levels of information, simulating data for entire systems, and generating a subset of quantities of interest conditioned on others. As a generative model, ACM-FD produces predictive samples, naturally supporting uncertainty quantification across all contexts. The contributions of our work are summarized as follows.

- **Multi-Functional Diffusion Framework:** we propose a multi-functional diffusion framework based on the Denoising Diffusion Probabilistic Model (DDPM) (Ho et al., 2020). By modeling noise as multiple Gaussian processes (GPs), we perform diffusion and denoising in functional spaces, enabling the generation of multiple functions required in multi-physics systems.
- **Innovative Denoising Loss:** we introduce a denoising loss that encapsulates all possible conditional parts within the system. During training, we randomly sample the conditioned part and fit the predicted noise for those parts to zero. This enables ACM-FD to flexibly generate function values conditioned on any other set of functions or quantities, allowing it to handle a wide range of tasks, such as forward prediction, inverse inference, and data simulation.
- **Efficient Training and Sampling:** To enable efficient training and sampling, and to flexibly handle irregularly sampled data that might come from real-world experiments and measurements, we use GPs to interpolate irregular function samples onto a grid. On the grid, we employ a multiplicative kernel to induce a Kronecker product structure within the kernel matrix. Leveraging the properties of the Kronecker product and tensor algebra, we avoid computing the full kernel matrix and its Cholesky decomposition, thereby substantially reducing the training and sampling costs.
- **Experiments:** We evaluated ACM-FD on three fundamental multi-physics systems, including Darcy flow, convection-diffusion, and torus fluid, with the number of involved functions ranging from three to seven. In twenty prediction tasks across the three systems, ACM-FD consistently achieved top-tier performance compared to state-of-the-art neural operators specifically trained for each task. Furthermore, we evaluated ACM-FD in data simulation. We compared with a popular variational auto-encoder approach. The data generated by ACM-FD not only adheres much more closely to the governing equations but also exhibits substantially greater diversity.

2. PRELIMINARIES

The denoising diffusion probabilistic model (DDPM) (Ho et al., 2020) is one of the most successful generative models. Given a collection of data instances, such as images, DDPM aims to capture the complex underlying distribution of these instances and generate new samples from the same distribution. To achieve this, DDPM specifies a forward diffusion process that gradually transforms each data instance \mathbf{x}_0 into Gaussian white noise. The forward process is modeled as a Gauss-Markov chain,

$$q(\mathbf{x}_0, \dots, \mathbf{x}_T) = q(\mathbf{x}_0) \prod_{t=1}^T q(\mathbf{x}_t | \mathbf{x}_{t-1}), \quad (1)$$

where $q(\mathbf{x}_0)$ represents the original data distribution, and each transition $q(\mathbf{x}_t | \mathbf{x}_{t-1}) = \mathcal{N}(\mathbf{x}_t | \sqrt{1 - \beta_t} \mathbf{x}_{t-1}, \beta_t \mathbf{I})$, with $\beta_t > 0$ as the noise level at step t . From this, it is straightforward to derive the relationship between the noisy instance \mathbf{x}_t and the original instance \mathbf{x}_0 ,

$$\mathbf{x}_t = \sqrt{\hat{\alpha}_t} \mathbf{x}_0 + \sqrt{1 - \hat{\alpha}_t} \boldsymbol{\xi}_t, \quad \boldsymbol{\xi}_t \sim \mathcal{N}(\cdot | 0, \mathbf{I}), \quad (2)$$

where $\hat{\alpha}_t = \prod_{j=1}^t \alpha_j$ and $\alpha_t = 1 - \beta_t$. As t increases, $\hat{\alpha}_t$ approaches zero, and $1 - \hat{\alpha}_t$ approaches 1, indicating that \mathbf{x}_t is gradually converging to a standard Gaussian random variable. When t becomes sufficiently large, we can approximately view \mathbf{x}_t as Gaussian white noise.

DDPM then learns to reverse this diffusion process to reconstruct the original instance \mathbf{x}_0 from the Gaussian white noise. Data generation, or sampling, is achieved by running this reversed process, which is often referred to as the denoising process. The reversed process is modeled as another Gauss-Markov chain, expressed as

$$p_{\Theta}(\mathbf{x}_T, \dots, \mathbf{x}_0) = p(\mathbf{x}_T) \prod_{t=1}^T p_{\Theta}(\mathbf{x}_{t-1} | \mathbf{x}_t), \quad (3)$$

where $p(\mathbf{x}_T) = \mathcal{N}(\mathbf{x}_T | \mathbf{0}, \mathbf{I})$, and Θ denotes the model parameters. DDPM uses the variational learning framework (Wainwright et al., 2008), which leads to matching each transition $p_{\Theta}(\mathbf{x}_{t-1} | \mathbf{x}_t)$ to the reversed conditional distribution from the forward diffusion process,

$$\begin{aligned} q(\mathbf{x}_{t-1} | \mathbf{x}_t, \mathbf{x}_0) \\ = \mathcal{N}\left(\mathbf{x}_{t-1} \middle| \frac{1}{\sqrt{1 - \beta_t}} \left(\mathbf{x}_t - \frac{\beta_t}{\sqrt{1 - \hat{\alpha}_t}} \boldsymbol{\xi}_t\right), \hat{\beta}_t \mathbf{I}\right), \end{aligned} \quad (4)$$

where $\hat{\beta}_t = \frac{1 - \hat{\alpha}_{t-1}}{1 - \hat{\alpha}_t} \beta_t$. Accordingly, DDPM employs a neural network Φ to approximate the noises $\boldsymbol{\xi}_t$; see (2). The training objective is to minimize the denoising loss, $\mathbb{E}_t \|\Phi_{\Theta}(\mathbf{x}_t, t) - \boldsymbol{\xi}_t\|^2$.

3. METHOD

We consider a multi-physics system involving a collection of M functions. These functions may represent initial and boundary conditions, source functions, parameter functions, system states and others. Our goal is to capture the underlying complex relationships between these functions and perform a wide range of prediction and simulation tasks, such as forward prediction of the system state given the initial condition, inverse inference about the systems parameters given observed states, joint simulation of all the functions, or conditional simulation of one set of functions based on another.

Many of these tasks involve mapping between functions, making neural operators (Li et al., 2020a; Lu et al., 2021; Kovachki et al., 2023) — a recently developed class of surrogate models — an appealing approach. However, most neural operators are trained for a single prediction task. To perform a different task, one would need to train another model from scratch. Additionally, these models generally lack uncertainty quantification, which is important for many applications. Furthermore, these models are unable to perform data generation tasks.

To address these issues, we propose AFML, an innovative generative model that can serve as a powerful and versatile probabilistic emulator for multi-physics systems.

3.1 Multi-Functional Diffusion

We first extend DDPM to enable functional data generation. To this end, we generalize the diffusion process in (2) to the functional space. Given a function instance $f_0(\cdot)$, we gradually transform it into a noise function via

$$f_t(\cdot) = \sqrt{\hat{\alpha}_t} f_0(\cdot) + \sqrt{1 - \hat{\alpha}_t} \boldsymbol{\xi}_t(\cdot), \quad (5)$$

where $f_t(\cdot)$ is the noisy version of f_0 at step t , and $\boldsymbol{\xi}_t(\cdot)$ is the noise function used to corrupt f_0 . To model the noise function, one can employ an expressive stochastic process. We choose to sample each noise function from a zero-mean Gaussian process (GP) (Rasmussen and Williams, 2006),

$$\boldsymbol{\xi}_t \sim \mathcal{GP}(\cdot | 0, \kappa(\mathbf{z}, \mathbf{z}')), \quad (6)$$

where $\kappa(\cdot, \cdot)$ is the covariance (kernel) function and \mathbf{z} and \mathbf{z}' denote the input locations of the function. When t becomes sufficiently large (i.e., $\hat{\alpha}_t \approx 0$), we can approximate $f_t \sim \mathcal{GP}(0, \kappa(\mathbf{z}, \mathbf{z}'))$, meaning it effectively turns into a noise function.

The actual data instance is the function sampled at a finite set of locations, $\mathbf{f}_0 = f_0(\mathcal{Z}) = (f_0(\mathbf{z}_1), \dots, f_0(\mathbf{z}_N))^\top$ where $\mathcal{Z} = \{\mathbf{z}_j | 1 \leq j \leq N\}$ are the sampling locations. Therefore, we only need to apply the diffusion process (5) to \mathcal{Z} (with the function values at all the other locations marginalized out), which yields:

$$\mathbf{f}_t = \sqrt{\hat{\alpha}_t} \mathbf{f}_0 + \sqrt{1 - \hat{\alpha}_t} \boldsymbol{\xi}_t, \quad \boldsymbol{\xi}_t \sim \mathcal{N}(\cdot | 0, \mathbf{K}), \quad (7)$$

where $\mathbf{f}_t = f_t(\mathcal{Z})$, $\boldsymbol{\xi}_t = \xi_t(\mathcal{Z})$, and $\mathbf{K} = \kappa(\mathcal{Z}, \mathcal{Z})$ is the covariance matrix at \mathcal{Z} .

Based on (7), we can derive the reversed conditional distribution,

$$\begin{aligned} q(\mathbf{f}_{t-1} | \mathbf{f}_t, \mathbf{f}_0) \\ = \mathcal{N} \left(\mathbf{f}_{t-1} \mid \frac{1}{\sqrt{1 - \beta_t}} \left(\mathbf{f}_t - \frac{\beta_t}{\sqrt{1 - \hat{\alpha}_t}} \boldsymbol{\xi}_t \right), \hat{\beta}_t \mathbf{K} \right). \end{aligned} \quad (8)$$

Comparing to (4), the only difference is that the identity matrix is replaced by the covariance matrix \mathbf{K} at the sampling locations \mathcal{Z} . We then use a similar strategy as in DDPM. We train a neural network Φ_Θ such that $\Phi_\Theta(\mathbf{f}_t, t, \mathcal{Z}) \approx \boldsymbol{\xi}_t$, and substitute the neural network's prediction for $\boldsymbol{\xi}_t$ in (8) to obtain $p_\Theta(\mathbf{x}_{t-1} | \mathbf{x}_t)$ for denoising and data sampling.

We next generalize to the multi-functional case. Given M functions of interest, $\mathcal{F} = \{f_0^1(\cdot), \dots, f_0^M(\cdot)\}$, we employ the same diffusion process as specified in (5) and (7) to transform each function into a noise function. Next, we use a single neural network to jointly recover or sample of all the functions, thereby capturing the complex and strong relationships among them. Specifically, we construct a network Φ_Θ that takes the step t , all the noisy function values sampled at t , and the sampling locations as the input, to predict the corresponding noises,

$$\phi_\Theta(\mathbf{f}_t^1, \dots, \mathbf{f}_t^M, t, \bar{\mathcal{Z}}) \approx (\boldsymbol{\xi}_t^1, \dots, \boldsymbol{\xi}_t^M), \quad (9)$$

where each $\mathbf{f}_t^k = f_t^k(\mathcal{Z}_k)$, $\boldsymbol{\xi}_t^k = \xi_t^k(\mathcal{Z}_k)$, $f_t^k(\cdot)$ is the noisy version of $f_0^k(\cdot)$ at step t , $\xi_t^k(\cdot)$ is the corresponding noise function that corrupts f_0^k to yield f_t^k , and \mathcal{Z}_k are the sampling locations of f_0^k , and $\bar{\mathcal{Z}} = \{\mathcal{Z}_k\}_{k=1}^M$.

3.2 Arbitrarily-Conditioned Denoising Loss

The design of our multi-functional denoising model (9) enables us to perform a wide range of conditional sampling and prediction tasks, beyond just functional data generation.

Specifically, let us denote an arbitrary set of conditioned function values as $\mathbf{F}^c = \{f_0^k(\mathcal{Z}_k^c) | k \in \mathcal{C}\}$, and the target function values to be generated as $\mathbf{F}^s = \{f_0^k(\mathcal{Z}_k^s) | k \in \mathcal{S}\}$. Note that \mathcal{C} and \mathcal{S} may overlap, provided that for any $f^k \in \mathcal{C} \cap \mathcal{S}$, the sampling locations do not, i.e., $\mathcal{Z}_k^c \cap \mathcal{Z}_k^s = \emptyset$. To generate \mathbf{F}^s conditioned on \mathbf{F}^c , we fix \mathbf{F}^c in the input to the network Φ_Θ , and vary only the noisy state associated with \mathbf{F}^s , denoted as \mathbf{F}_t^s . The input to Φ consists of $\mathbf{F}^c \cup \mathbf{F}_t^s \cup \{t, \bar{\mathcal{Z}}\}$. We use the predicted noise corresponding to \mathbf{F}_t^s to sample \mathbf{F}_{t-1}^s , following the denoising process. This procedure is repeated until $t = 0$, resulting in a sample for \mathbf{F}^s . The sampling process is summarized in Algorithm 2.

By varying the choices of \mathbf{F}^c and \mathbf{F}^s , our model can perform a wide variety of data generation and prediction tasks. When $\mathbf{F}^c = \emptyset$, the model jointly samples the M target functions at the specified input locations. When $\mathbf{F}^c \neq \emptyset$ and $\mathcal{C} \cap \mathcal{S} = \emptyset$, the model generates one set of functions conditioned on the other, supporting various forward prediction and inverse inference tasks. For instance, by setting \mathcal{C} to include initial conditions or current and/or past system states and source functions, and \mathcal{S} to the future system states, the model performs forward prediction. Alternatively, if the observed system states are included in \mathcal{C} and \mathcal{S} corresponds to initial/boundary conditions, system parameters, or past states, the model carries out inverse inference. Even for the same type of tasks, the functions and the number of functions in \mathcal{C} , as well as the number of sampling locations in \mathcal{Z}_k^c , can be adjusted to accommodate different levels of available information

for prediction. When $\mathcal{C} \cap \mathcal{S} \neq \emptyset$, the model performs not only conditional sampling of other functions but also completion of the observed functions at new locations. All tasks are executed using a single model, Φ_Θ , following the same denoising process. One can generate as many predictive samples as needed, naturally supporting uncertainty quantification in any context. Thereby, our method offers a versatile probabilistic surrogate for multi-physics emulation.

However, to build a well-performing model, training Φ to predict all the noises as specified in (9) is far from sufficient, because it only handles unconditioned sampling. To make our model capable of handling all kinds of tasks, we introduce a random mask variable, $\mathcal{H} = \{\mathbf{h}^1, \dots, \mathbf{h}^M\}$. Each element in \mathcal{H} is binary, indicating whether the corresponding function value is conditioned or to be sampled. If a function value is conditioned, then it should remain fixed as a constant input to Φ , and correspondingly, the predicted noise for that value should be zero, since it is never corrupted by any noise. Accordingly, we introduce a new denoising loss,

$$\begin{aligned} \mathcal{L}(\Theta) & \\ &= \mathbb{E}_t \mathbb{E}_{p(\mathbf{H})} \left\| \Phi_\Theta(\widehat{\mathbf{f}}_t^1, \dots, \widehat{\mathbf{f}}_t^M, t, \bar{\mathcal{Z}}) - (\widehat{\boldsymbol{\xi}}_t^1, \dots, \widehat{\boldsymbol{\xi}}_t^M) \right\|^2, \end{aligned} \quad (10)$$

where for each $1 \leq k \leq M$,

$$\begin{aligned} \widehat{\mathbf{f}}_t^k &= \mathbf{f}_0^k \circ \mathbf{h}^k + \mathbf{f}_t^k \circ (\mathbf{1} - \mathbf{h}^k), \\ \widehat{\boldsymbol{\xi}}_t^k &= \mathbf{0} \circ \mathbf{h}^k + \boldsymbol{\xi}_t^k \circ (\mathbf{1} - \mathbf{h}^k). \end{aligned} \quad (11)$$

Here \mathbf{f}_0^k is the original function instance sampled at the specified locations \mathcal{Z}^k , $\mathbf{f}_t^k = \sqrt{\widehat{\alpha}_t} \mathbf{f}_0^k + \sqrt{1 - \widehat{\alpha}_t} \boldsymbol{\xi}_t^k$ is the noisy version of \mathbf{f}_0^k at step t , and \circ denotes the element-wise product. The choice of $p(\mathcal{H})$ is flexible. Without any prior knowledge or preferences, we can simply set $p(\mathcal{H}) = \prod_{h \in \mathcal{H}} \text{Bernoulli}(h|0.5)$. Our denoising loss (10) accommodates all possible conditional components for conditioned sampling as well as unconditioned sampling (i.e., $\mathcal{H} = \{0\}$), allowing our model to be trained for all kinds of tasks. We use stochastic training, which involves randomly sampling the mask \mathcal{H} , applying it to the function and noise instances as specified in (11), and computing the stochastic gradient $\nabla_\Theta \left\| \Phi_\Theta(\widehat{\mathbf{f}}_t^1, \dots, \widehat{\mathbf{f}}_t^M, t, \bar{\mathcal{Z}}) - (\widehat{\boldsymbol{\xi}}_t^1, \dots, \widehat{\boldsymbol{\xi}}_t^M) \right\|^2$ to update the model parameters Θ .

3.3 Efficient Training And Sampling

The training and generation with our model requires repeatedly sampling noise functions from GPs, as specified in (7). The sampling necessitates the Cholesky decomposition of the covariance matrix \mathbf{K} at the input locations, which has a time complexity of $\mathcal{O}(N^3)$, where N is the number of input locations. When N is large, the computation becomes prohibitively expensive or even infeasible. However, large values of N is not uncommon in realistic systems. For instance, generating a 2D function sample on a 128×128 mesh results in $N = 128 \times 128 = 16,384$.

To address this challenge, we use a multiplicative kernel to model the noise function. Given the input dimension D , we define the kernel as

$$\kappa(\mathbf{z}, \mathbf{z}') = \prod_{d=1}^D \kappa(z_d, z'_d). \quad (12)$$

Notably, the widely used Square Exponential (SE) kernel already exhibits this structure. We position the sampling locations for each target function $f_0^k(\cdot)$ on an $m_1 \times \dots \times m_D$ mesh, denoted as $\mathcal{Z}_k = \gamma_1 \times \dots \times \gamma_D$, where \times denotes the Cartesian product, and each γ_d ($1 \leq d \leq D$) comprises the m_d input locations within dimension d .

Algorithm 1 Training($\mathcal{Z}_1, \dots, \mathcal{Z}_M, p(\mathcal{H})$)

- 1: **repeat**
- 2: Sample instances of the M functions of interest over meshes $\{\mathcal{Z}_k\}_{k=1}^M$, denoted by $\{\mathbf{f}_0^1, \dots, \mathbf{f}_0^M\}$.
- 3: $t \sim \text{Uniform}(1, \dots, T)$
- 4: Sample M noise functions from GPs over $\{\mathcal{Z}_k\}_{k=1}^M$, denoted by $\{\boldsymbol{\xi}_t^1, \dots, \boldsymbol{\xi}_t^M\}$, where each $\boldsymbol{\xi}_t^k$ corresponds to \mathbf{f}_t^k , using (12) and (13)
- 5: Sample the mask $\mathcal{H} = \{\mathbf{h}^1, \dots, \mathbf{h}^M\} \sim p(\mathcal{H})$
- 6: Take gradient descent step on

$$\nabla_{\Theta} \left\| \Phi_{\Theta}(\widehat{\mathbf{f}}_t^1, \dots, \widehat{\mathbf{f}}_t^M, t, \overline{\mathcal{Z}}) - (\widehat{\boldsymbol{\xi}}_t^1, \dots, \widehat{\boldsymbol{\xi}}_t^M) \right\|^2,$$

where $\overline{\mathcal{Z}} \triangleq \{\mathcal{Z}_k\}_{k=1}^M$, each $\widehat{\mathbf{f}}_t^k$ and $\widehat{\boldsymbol{\xi}}_t^k$ ($1 \leq k \leq M$) are masked instances as defined in (11).

- 7: **until** Converged
-

Algorithm 2 Generation (conditioned: \mathbf{F}^c , target: \mathbf{F}^s , target locations: $\overline{\mathcal{Z}}^s$, all locations: $\overline{\mathcal{Z}} = \{\mathcal{Z}_k\}$)

- 1: Sample noise functions from GPs over $\overline{\mathcal{Z}}$ using (12) and (13), denoted as $\overline{\boldsymbol{\xi}}$
- 2: $\mathbf{F}_T^s \leftarrow$ Subset of $\overline{\boldsymbol{\xi}}$ at $\overline{\mathcal{Z}}^s$
- 3: **for** $t = T, \dots, 1$ **do**
- 4: $\overline{\boldsymbol{\epsilon}} \leftarrow \mathbf{0}$
- 5: **if** $t > 1$ **then**
- 6: Re-sample $\overline{\boldsymbol{\xi}}$ following STEP 1
- 7: $\overline{\boldsymbol{\epsilon}} \leftarrow$ Subset of $\overline{\boldsymbol{\xi}}$ at $\overline{\mathcal{Z}}^s$
- 8: **end if**
- 9: $\overline{\boldsymbol{\xi}}_t^s \leftarrow \Phi_{\Theta}(\mathbf{F}^c \cup \mathbf{F}_t^s, t, \overline{\mathcal{Z}})$
- 10: $\boldsymbol{\xi}_t^s \leftarrow$ Subset of $\overline{\boldsymbol{\xi}}_t^s$ at $\overline{\mathcal{Z}}^s$
- 11: Generate sample

$$\mathbf{F}_{t-1}^s = \frac{1}{\sqrt{1 - \beta_t}} \left(\mathbf{F}_t^s - \frac{\beta_t}{\sqrt{1 - \alpha_t}} \overline{\boldsymbol{\xi}}_t^s \right) + \widehat{\beta}_t \overline{\boldsymbol{\epsilon}}$$

- 12: **end for**
 - 13: **return** \mathbf{F}_0^s
-

From the multiplicative kernel (12), we can induce a Kronecker product in the covariance matrix, namely $\mathbf{K} \triangleq \kappa(\mathcal{Z}_k, \mathcal{Z}_k) = \mathbf{K}_1 \otimes \dots \otimes \mathbf{K}_D$ where each $\mathbf{K}_d = \kappa(\gamma_d, \gamma_d)$. We then perform the Cholesky decomposition on each local kernel matrix, yielding $\mathbf{K}_d = \mathbf{L}_d \mathbf{L}_d^{\top}$. Utilizing the properties of Kronecker products, we can derive that $\mathbf{K}^{-1} = (\mathbf{L}_1^{-1})^{\top} \mathbf{L}_1^{-1} \otimes \dots \otimes (\mathbf{L}_D^{-1})^{\top} \mathbf{L}_D^{-1} = \mathbf{A}^{\top} \mathbf{A}$ where $\mathbf{A} = \mathbf{L}_1^{-1} \otimes \dots \otimes \mathbf{L}_D^{-1}$. Consequently, to generate a sample of $\boldsymbol{\xi}_t$ on the mesh, we can first sample a standard Gaussian variable $\boldsymbol{\eta} \sim \mathcal{N}(\mathbf{0}, \mathbf{I})$, and then obtain the sample as $\text{vec}(\boldsymbol{\xi}_t) = \mathbf{A}^{\top} \boldsymbol{\eta}$ where $\text{vec}(\cdot)$ denotes the vectorization. Note that $\boldsymbol{\xi}_t$ is a $m_1 \times \dots \times m_D$ tensor. However, directly computing the Kronecker product in \mathbf{A} and then evaluating $\mathbf{A}^{\top} \boldsymbol{\eta}$ can be computationally expensive, with a time complexity of $\mathcal{O}(\overline{m}^2)$, where $\overline{m} = \prod_d m_d$ represents the total number of the mesh points. To reduce the cost, we use tensor algebra (Kolda, 2006) to compute the Tucker product instead, which gives the same result without explicitly computing the Kronecker product,

$$\boldsymbol{\xi}_t^k = \Pi \times_1 \mathbf{L}_1^{-1} \times_2 \dots \times_D \mathbf{L}_D^{-1}, \quad (13)$$

where we reshape $\boldsymbol{\eta}$ into an $m_1 \times \dots \times m_D$ tensor Π , and \times_k is the tensor-matrix product along mode k . The time complexity of this operation becomes $\mathcal{O}(\overline{m}(\sum_d m_d))$. Overall, this approach avoids computing the full covariance matrix \mathbf{K} for all the mesh points along with its Cholesky decomposition, which would require

$\mathcal{O}(\bar{m}^3)$ time and $\mathcal{O}(\bar{m}^2)$ space complexity. Instead we only compute the local kernel matrix for each input dimension. For example, when using a 128×128 mesh, the full covariance matrix would be $128^2 \times 128^2$, which is highly expensive to compute. In contrast, our approach requires the computation of only two local kernel matrices, each of size 128×128 . Our approach further uses the Tucker product to compute the sample (see (13)), thereby avoiding the computationally expensive Kronecker product. As a result, the overall time and space complexity is reduced to $\mathcal{O}(\sum_d m_d^3 + \bar{m}(\sum_d m_d))$ and $\mathcal{O}(\sum_d m_d^2 + \bar{m})$, respectively.

In cases where the data is irregularly and sparsely sampled — often the case with practical observation or measurement data — we employ a GP model to interpolate the function values onto a grid. This allows us to efficiently train and sample using the aforementioned approach. Empirically, we have found that this straightforward strategy demonstrates robust performance, often surpassing alternative approaches such as attention mechanisms (see Section 5.1). Finally, we summarize the training and generation of ACM-FD in Algorithm 1 and 2, respectively.

4. RELATED WORK

Generative models have been studied for a long time. One class is the likelihood-based approach, which uses neural networks to approximate the probability density function, and maximize the likelihood of the observed data under the model. This category includes auto-regressive models (Larochelle and Murray, 2011; Germain et al., 2015; Van Den Oord et al., 2016), variational auto-encoders (Kingma and Welling, 2013; Rezende et al., 2014), normalization flows (Dinh et al., 2014, 2016; Papamakarios et al., 2017), and energy-based models LeCun et al. (2006); Gutmann and Hyvärinen (2010); Song and Kingma (2021), and others. A second class is implicit generative models (Mohamed and Lakshminarayanan, 2016), which transforms a random variable drawn from a standard distribution (*e.g.*, Gaussian) into a new variable, typically, via neural networks, resulting in a complex implicit density model. Typical examples of such methods include Generative Adversarial Networks (GAN) and their variants Goodfellow et al. (2014); Salimans et al. (2016); Arjovsky et al. (2017).

The recent DDPM work (Ho et al., 2020) is a break-through, which specifies a probability-path (diffusion process) that progressively converts data instances into noise and then learns to reverse this path. Numerous subsequent works have built upon this direction, such as score-based diffusion via SDEs (Song et al., 2021b), denoising diffusion implicit models (DDIM) (Song et al., 2021a), flow-matching (Lipman et al., 2022; Klein et al., 2023) fast sampling (Salimans and Ho, 2022; Kong and Ping, 2021; Zhang and Chen, 2023; Shih et al., 2023), latent diffusion (Rombach et al., 2022; Avrahami et al., 2023), and others. The most recent work (Zhang and Wonka, 2024) proposed functional diffusion under the DDIM framework. The key difference is that it focuses on single-function generation and does not address multi-functional scenarios or diverse conditional sampling tasks, as we do. Another notable recent work by Kerrigan et al. (2024) extends the flow-matching framework, based on neural Ordinary Differential Equations (Chen et al., 2018), for functional generation. In addition to being based on different generative modeling frameworks, our work primarily differs in that we train a single model to handle a diverse set of conditioned and unconditioned functional sampling tasks, whereas (Kerrigan et al., 2024) focuses on a single task.

Neural operator (NOs) are emerging as a prominent research area in ML-based surrogate models. Their goal is to learn function-to-function mappings from data, primarily for estimating PDE operators from simulation data and performing forward predictions of PDE solutions given new inputs. Important works include Fourier Neural Operators (FNO) (Li et al., 2022a) and Deep Operator Net (DONet) (Lu et al., 2021), which have demonstrated promising prediction accuracy across various benchmark PDEs (Lu et al., 2022), such as Burger’s equation, Darcy-flow and Navier-Stoke (NS) equations. Many NO models have been developed based on FNO and DONet. For example, Gupta et al. (2021) contributed with multiwavelet transformations for the operator’s kernel. Lu et al. (2022) proposed POD-DONet to enhance the stability of DONet by replacing the trunk net with POD (PCA) bases constructed from data. A recent line of research attempts to build neural operators using attention/transformer architectures, such as (Cao, 2021; Li et al., 2022b; Hao et al., 2023). Additionally, recent advances in kernel operator learning strategies have been made by Long et al. (2022) and Batlle et al. (2023). A recent review of NOs can be found in (Kovachki et al., 2023).

5. EXPERIMENTS

For evaluation, we considered three fundamental multi-physics systems: **Darcy Flow**: a single-phase 2D Darcy flow system that involves three functions: the permeability field a , the flow pressure u , and the source term f . **Convection Diffusion**: a 1D convection-diffusion system that involves three spatial-temporal functions: the scalar field of the quantity of interest u , the velocity field v , and the source function s . **Torus Fluid**: a viscous, incompressible fluid in the unit torus, for which we are interested in seven functions, including the source function f , the initial vorticity field w_0 , and the vorticity fields w_1, \dots, w_5 at five different time steps $t = 2, 4, 6, 8, 10$.

The details about these systems, along with the preparation of training and test data, are provided in Appendix Section A.

Table 1: Relative L_2 Error For Various Prediction Tasks, With Training And Test Functions Sampled On Regular Meshes. The Results Were Averaged Over Five runs. D-F, C-D And T-F Are Short For Darcy Fow, Convection Diffusion, And Torus Fluid Systems.

Dataset	Task(s)	ACM-FD	FNO	GNOT	DON	PODDON
D-F	f, u to a	1.32e-02 (2.18e-04)	1.88e-02 (1.66e-04)	1.35e-01 (6.57e-05)	2.38e-02 (3.45e-04)	1.56e-02 (1.44e-04)
	a, u to f	1.59e-02 (1.59e-04)	2.37e-02 (1.87e-04)	1.00e+00 (0.00e+00)	3.76e-02 (7.75e-04)	4.63e-02 (1.21e-03)
	a, f to u	1.75e-02 (4.16e-04)	6.29e-02 (4.18e-04)	6.09e-01 (2.40e-01)	6.05e-02 (7.17e-04)	6.80e-02 (2.16e-04)
	u to a	3.91e-02 (7.08e-04)	5.57e-02 (4.16e-04)	1.35e-01 (1.99e-04)	5.08e-02 (5.91e-04)	4.09e-02 (4.18e-04)
	u to f	3.98e-02 (6.45e-04)	5.50e-02 (5.47e-04)	9.99e-01 (7.48e-04)	6.46e-02 (1.13e-04)	6.37e-02 (1.03e-03)
C-D	s, u to v	2.17e-02 (4.53e-04)	4.50e-02 (3.89e-04)	3.26e-02 (3.41e-03)	3.64e-02 (5.07e-04)	4.62e-02 (2.00e-04)
	v, u to s	5.45e-02 (1.40e-03)	7.93e-02 (8.48e-04)	1.22e-01 (1.91e-03)	7.04e-02 (7.53e-04)	7.57e-02 (4.09e-04)
	v, s to u	1.60e-02 (2.15e-04)	7.26e-02 (2.16e-04)	5.80e-03 (1.51e-04)	7.86e-02 (7.42e-04)	1.72e-01 (1.17e-03)
	u to v	2.66e-02 (3.08e-04)	5.90e-02 (8.22e-04)	6.69e-02 (3.66e-03)	4.55e-02 (6.09e-04)	5.38e-02 (5.29e-04)
	u to s	6.06e-02 (2.54e-04)	1.16e-01 (5.63e-04)	1.85e-01 (2.84e-03)	9.65e-02 (5.52e-04)	1.03e-01 (1.29e-03)
T-F	w_0, w_5 to w_1	2.73e-02 (4.78e-03)	1.28e-02 (2.38e-04)	2.40e-02 (8.74e-04)	6.32e-02 (2.72e-04)	6.06e-02 (2.91e-04)
	w_0, w_5 to w_2	2.43e-02 (1.60e-03)	2.08e-02 (9.80e-05)	4.00e-02 (5.92e-04)	7.69e-02 (4.41e-04)	7.71e-02 (1.63e-04)
	w_0, w_5 to w_3	2.43e-02 (3.17e-03)	2.33e-02 (1.83e-04)	4.74e-02 (1.23e-03)	7.34e-02 (2.88e-04)	7.38e-02 (2.92e-04)
	w_0, w_5 to w_4	1.68e-02 (1.81e-03)	1.41e-02 (1.17e-04)	3.95e-02 (6.73e-04)	5.57e-02 (1.73e-04)	5.38e-02 (2.18e-04)
	w_0, w_5 to f	1.63e-02 (1.49e-03)	1.79e-02 (3.04e-04)	5.91e-02 (4.01e-03)	4.77e-02 (5.56e-04)	4.94e-02 (9.02e-04)
	w_0, f to w_1	3.10e-02 (4.08e-03)	9.68e-03 (3.22e-04)	2.09e-02 (3.62e-04)	6.08e-02 (3.14e-04)	5.54e-02 (6.45e-04)
	w_0, f to w_2	3.28e-02 (4.79e-03)	1.70e-02 (3.51e-04)	4.15e-02 (8.21e-04)	7.73e-02 (6.18e-04)	7.40e-02 (2.01e-04)
	w_0, f to w_3	3.49e-02 (2.38e-03)	2.38e-02 (8.37e-05)	5.61e-02 (8.23e-04)	8.82e-02 (4.45e-04)	8.60e-02 (5.16e-04)
	w_0, f to w_4	3.34e-02 (3.87e-03)	3.10e-02 (1.26e-04)	6.97e-02 (1.62e-03)	1.02e-01 (7.28e-04)	9.74e-02 (4.21e-04)
w_0, f to w_5	3.26e-02 (2.13e-03)	3.81e-02 (2.01e-04)	8.35e-02 (7.33e-04)	1.21e-01 (8.20e-04)	1.16e-01 (8.07e-04)	

5.1 Predictive Performance Across Various Tasks

We first examined performance of ACM-FD across a variety of prediction tasks, each predicting one function using another set of functions. These tasks address a wide range of forward prediction and inverse inference problems. For example, in the case of *Darcy flow*, predicting the pressure field u given the permeability field a and the forcing term f is a forward prediction task, while predicting a from u and f , or predicting f from u and a , typically represents inverse problems. Due to the versatility of ACM-FD, a single trained model can be used to perform all these tasks.

Methods. We compared with the following popular and state-of-the-art operator learning methods: (1) Fourier Neural Operator (FNO) (Li et al., 2020b), which performs channel lifting, followed by a series of Fourier layers that execute linear functional transformations using the fast Fourier transform and then apply nonlinear transformations, ultimately culminating in a projection layer that produces the prediction. (2) Deep Operator Net (DON) (Lu et al., 2021), which employs a branch-net and a trunk-net to extract representations of the input functions and querying locations, producing the prediction by the dot product between the two representations. (3) PODDON (Lu et al., 2022), a variant of DON where the trunk-net is replaced by the

POD (PCA) bases extracted from the training data. (4) GNOT (Hao et al., 2023), a transformer-based neural operator that uses cross-attention layers to aggregate multiple input functions’ information for prediction. We utilized the original implementation of each competing method. Our method, ACM-FD, was implemented with PyTorch. For GP noise function sampling and interpolation of irregularly sampled functions, we used the Square-Exponential (SE) kernel. In the experiments, we used FNO to construct our denoising network Φ_{Θ} . Thereby, our comparison with FNO can exclude the factors from the architecture design.

Setting. We employed two evaluation settings for each task. In the first setting, all functions are sampled on a regular 64×64 grid, while the second setting samples each function from random input locations within the domain, with the number of samples varying from 1,200 to 1,500. To enable FNO and PODDON to train with irregularly sampled data, we used `scipy.interpolate.griddata` routine to interpolate the sampled functions onto a 64×64 grid. Note that DON and GNOT can directly process irregularly sampled data. For both the regularly and irregularly sampled settings, we utilized 1,000 instances for training, 100 instances for validation, and 200 instances for testing. Hyperparameter tuning was performed using the validation set. The details are provided in Appendix Section B. Following the evaluation procedure in (Lu et al., 2022), for each method, we selected the optimal hyperparameters, and then conducted stochastic training for five times, reporting the average relative L_2 test error along with the standard deviation. The results for the regularly-sampled case and irregularly-sampled case are presented in Table 1 and 2, respectively.

Result. As we can see, ACM-FD consistently achieved top-tier predictive performance across all tasks. In the regularly-sampled setting, ACM-FD outperforms FNO in all tasks for both Darcy Flow and Convection Diffusion. In the Torus Fluid system, while ACM-FD ranks second, its performance remains close to that of FNO. In the irregularly sampled setting, ACM-FD consistently outperforms all competing methods, often by a large margin. It is worth noting that GNOT is a transformer based approach, and by using the cross-attention layers, GNOT can flexibly handle irregularly sampled data, without the need to conduct explicit interpolation. However, GNOT still consistently performs worse than ACM-FD across all the tasks, despite being specifically tuned for each task. A similar observation holds for DON. These results demonstrate the superior performance and versatility of ACM-FD.

5.2 Generation Performance

We then evaluated the generation performance of ACM-FD by using it to generate instances of all relevant functions for the *Darcy Flow* and *Convection Diffusion* systems. We compared ACM-FD with a popular version of the Variational Auto-Encoder (VAE), known as β -VAE (Higgins et al., 2022), where β controls the regularization strength from the prior. The encoder network was built using a series of convolutional layers, while the decoder network was constructed as the transpose of these layers. For training and hyperparameter tuning of β -VAE, we used the same training and validation sets as those used by ACM-FD in Section 5.1. The details are provided in Section B. To let β -VAE train with irregularly-sampled data, we also applied `scipy.interpolate.griddata` for interpolation.

We used two metrics to evaluate the quality of the generated data. The first is the *equation error*, which measures how well the generated data adheres to the governing equations of the system. To calculate this error, for each group of sampled source function, parameter function, and/or initial conditions, we ran the numerical solver (the same one used to generate the training data) to solve the governing equation(s), and then computed the relative L_2 error between the generated solution and the numerical solution. The second metric is the Mean-Relative-Pairwise-Distance (MRPD), which measures the diversity of the generated data and is commonly used in the evaluation of generative models (Yuan and Kitani, 2020; Barquero et al., 2023; Tian et al., 2024).

For each system, we generated 1,000 sets of the relevant functions. The average equation error and MRPD are presented in Table 3. As shown, the functions generated by ACM-FD consistently exhibit relatively small equation errors, indicating a strong alignment with the physical laws governing each system. In contrast, the equation errors for the data generated by β -VAE are much larger, often by an order of magnitude. Furthermore, the data generated by ACM-FD demonstrates a higher MRPD than those from β -VAE, indicating better

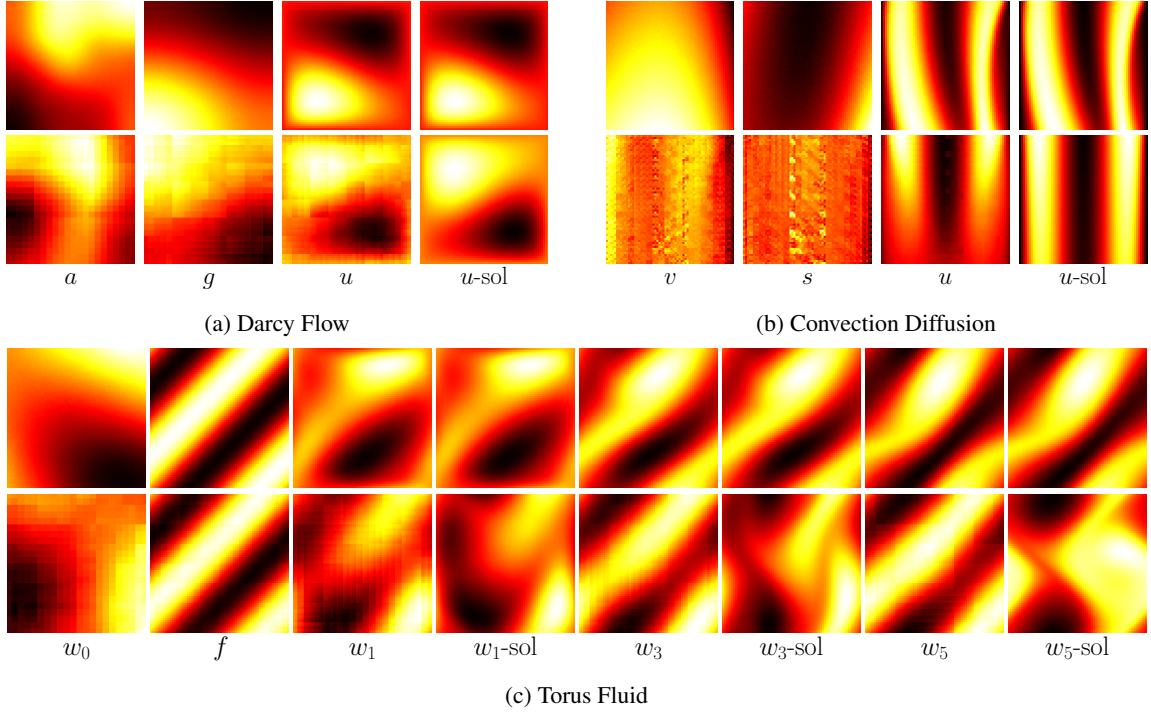


Figure 1: Generated Function Instances By ACM-FD (top row) And By β -VAE (Second Row). "-sol" Means The Numerical Solution Provided By The Numerical Solvers Given The Other Functions.

Table 2: Relative L_2 Error For Various Prediction Tasks, With Irregularly Sampled Training And Test Functions. The Results Were Averaged Over Five Runs.

System	Task(s)	ACM-FD	FNO	GNOT	DON	PODDON
D-F	f, u to a	1.35e-02 (3.33e-04)	2.79e-02 (2.89e-04)	1.35e-01 (2.18e-04)	3.39e-02 (6.71e-04)	3.59e-02 (8.51e-04)
	a, u to f	1.08e-02 (1.11e-02)	2.28e-02 (2.21e-02)	1.00e+00 (1.00e+00)	3.23e-02 (3.26e-02)	4.28e-02 (4.16e-02)
	a, f to u	1.33e-02 (8.12e-05)	4.49e-02 (4.79e-04)	9.99e-01 (9.27e-04)	5.34e-02 (3.85e-04)	6.58e-02 (7.26e-04)
	u to a	3.82e-02 (8.35e-04)	5.91e-02 (5.68e-04)	1.35e-01 (9.39e-05)	9.42e-02 (3.15e-03)	1.01e-01 (1.02e-03)
	u to f	3.77e-02 (4.45e-04)	6.07e-02 (5.58e-04)	9.99e-01 (7.53e-04)	1.01e-01 (3.26e-03)	9.47e-02 (1.34e-03)
C-D	s, u to v	2.65e-02 (7.79e-04)	5.55e-02 (6.98e-04)	1.05e-01 (2.19e-03)	4.37e-02 (2.19e-04)	5.91e-02 (9.05e-04)
	v, u to s	5.87e-02 (1.29e-03)	9.87e-02 (9.71e-04)	1.46e-01 (2.24e-03)	9.01e-02 (3.01e-03)	1.18e-01 (1.06e-03)
	v, s to u	3.45e-02 (3.87e-04)	6.64e-02 (6.63e-05)	2.40e-02 (4.67e-04)	7.59e-02 (2.76e-04)	2.17e-01 (6.16e-04)
	u to v	3.11e-02 (2.06e-04)	7.21e-02 (1.64e-03)	1.86e-01 (1.64e-02)	6.03e-02 (1.86e-03)	7.79e-02 (1.43e-03)
	u to s	6.34e-02 (8.90e-04)	1.36e-01 (2.24e-03)	2.04e-01 (6.26e-03)	1.22e-01 (3.56e-03)	1.77e-01 (3.13e-03)
T-F	w_0, w_5 to w_1	1.78e-02 (1.47e-03)	4.66e-02 (1.18e-03)	6.36e-02 (1.36e-03)	7.72e-02 (8.98e-04)	8.97e-02 (8.82e-04)
	w_0, w_5 to w_2	1.52e-02 (5.54e-04)	5.10e-02 (8.67e-04)	7.81e-02 (1.10e-03)	9.04e-02 (4.75e-04)	1.05e-01 (1.10e-03)
	w_0, w_5 to w_3	1.67e-02 (1.75e-03)	5.42e-02 (4.75e-04)	8.34e-02 (8.63e-04)	8.76e-02 (4.50e-04)	1.05e-01 (9.14e-04)
	w_0, w_5 to w_4	1.34e-02 (1.47e-03)	4.67e-02 (2.52e-04)	7.06e-02 (4.67e-04)	7.12e-02 (2.48e-04)	8.60e-02 (5.36e-04)
	w_0, w_5 to f	1.45e-02 (5.65e-04)	5.92e-02 (3.72e-04)	8.56e-02 (2.48e-03)	6.74e-02 (7.74e-04)	9.62e-02 (9.64e-04)
	w_0, f to w_1	1.96e-02 (1.97e-03)	4.32e-02 (1.98e-04)	5.89e-02 (7.27e-04)	7.72e-02 (5.28e-04)	8.68e-02 (8.65e-04)
	w_0, f to w_2	2.10e-02 (2.17e-03)	4.75e-02 (5.11e-04)	7.35e-02 (1.73e-03)	9.78e-02 (1.26e-03)	1.12e-01 (1.05e-03)
	w_0, f to w_3	2.03e-02 (1.50e-03)	5.39e-02 (2.97e-04)	9.73e-02 (1.86e-03)	1.13e-01 (6.47e-04)	1.31e-01 (6.74e-04)
	w_0, f to w_4	2.13e-02 (1.17e-03)	6.07e-02 (1.02e-03)	1.03e-01 (2.57e-03)	1.34e-01 (1.19e-03)	1.49e-01 (1.11e-03)
	w_0, f to w_5	2.51e-02 (1.39e-03)	6.66e-02 (8.54e-04)	1.10e-01 (5.86e-03)	1.64e-01 (2.67e-03)	1.76e-01 (1.53e-03)

Table 3: Equation Error And Diversity Of Generated Data For The Whole System. D-F, C-D, And T-F Are Short For Darcy Flow, Convection Diffusion, And Torus Fluid, Respectively. MRPD Is Short For Mean Relative Pairwise Distance.

System (setting)	Task(s)	ACM-FD	β -VAE
D-F (Regular)	Equation Error	0.0576	0.265
	MRPD	1.15	0.932
C-D (Regular)	Equation Error	0.114	0.282
	MRPD	1.00	0.879
T-F (Regular)	Equation Error	0.0273	0.737
	MRPD	0.8042	0.524
D-F (Irregular)	Equation Error	0.0427	0.32
	MRPD	1.52	0.928
C-D (Irregular)	Equation Error	0.065	0.285
	MRPD	1.49	0.949
T-F (Irregular)	Equation Error	0.0221	0.741
	MRPD	0.916	0.4907

diversity among the generated function instances. Overall, these results suggest that ACM-FD produces not only reliable but also diverse multi-physics data.

Next, we investigated the functions generated by each method. Figure 1 illustrates a set of functions randomly generated by ACM-FD and β -VAE for each system. More examples are provided in Appendix Figure 2. Our method’s generated solutions are highly consistent with the numerical solutions, accurately capturing both the global structures and finer details. In contrast, the solutions produced by β -VAE often fail to capture local details (see Fig. 1a for u and Fig. 1c for w_1) or significantly deviate from the numerical solution in terms of overall shape (see Fig. 1b for u and Fig. 1c for w_3).

In addition, other functions generated by β -VAE, such as (a, f) for Darcy Flow and (v, s) for Convection Diffusion, appear quite rough and do not align well with the corresponding function families (see Appendix Section A). This might be due to that β -VAE is unable to capture the correlations between function values across different input locations. In contrast, ACM-FD introduces GP noise functions and performs diffusion and denoising within the functional space. As a result, ACM-FD is flexible enough to effectively capture the diverse correlations between function values. Overall, these results confirm the advantages of our method in multi-physics data generation.

6. CONCLUSION

We have presented ACM-FD, a novel probabilistic generative model designed for multi-physics emulation. ACM-FD can perform arbitrarily-conditioned multi-function sampling and has demonstrated potential in several classical systems. In future work, we plan to extend our investigations into more complex multi-physics systems and explore alternative architecture designs to further enhance its capabilities.

References

- Martin Arjovsky, Soumith Chintala, and Léon Bottou. Wasserstein generative adversarial networks. In *International conference on machine learning*, pages 214–223. PMLR, 2017.
- Omri Avrahami, Ohad Fried, and Dani Lischinski. Blended latent diffusion. *ACM transactions on graphics (TOG)*, 42(4):1–11, 2023.
- German Barquero, Sergio Escalera, and Cristina Palmero. Belfusion: Latent diffusion for behavior-driven human motion prediction. In *Proceedings of the IEEE/CVF International Conference on Computer Vision*, pages 2317–2327, 2023.
- Pau Batlle, Matthieu Darcy, Bamdad Hosseini, and Houman Owhadi. Kernel methods are competitive for operator learning. *arXiv preprint arXiv:2304.13202*, 2023.

- Shuhao Cao. Choose a transformer: Fourier or galerkin. Advances in neural information processing systems, 34:24924–24940, 2021.
- Ricky TQ Chen, Yulia Rubanova, Jesse Bettencourt, and David K Duvenaud. Neural ordinary differential equations. Advances in neural information processing systems, 31, 2018.
- Laurent Dinh, David Krueger, and Yoshua Bengio. Nice: Non-linear independent components estimation. arXiv preprint arXiv:1410.8516, 2014.
- Laurent Dinh, Jascha Sohl-Dickstein, and Samy Bengio. Density estimation using real nvp. arXiv preprint arXiv:1605.08803, 2016.
- Mathieu Germain, Karol Gregor, Iain Murray, and Hugo Larochelle. Made: Masked autoencoder for distribution estimation. In International conference on machine learning, pages 881–889. PMLR, 2015.
- Ian Goodfellow, Jean Pouget-Abadie, Mehdi Mirza, Bing Xu, David Warde-Farley, Sherjil Ozair, Aaron Courville, and Yoshua Bengio. Generative adversarial nets. In Advances in neural information processing systems, pages 2672–2680, 2014.
- Gaurav Gupta, Xiongye Xiao, and Paul Bogdan. Multiwavelet-based operator learning for differential equations. Advances in neural information processing systems, 34:24048–24062, 2021.
- Michael Gutmann and Aapo Hyvärinen. Noise-contrastive estimation: A new estimation principle for unnormalized statistical models. In Proceedings of the thirteenth international conference on artificial intelligence and statistics, pages 297–304. JMLR Workshop and Conference Proceedings, 2010.
- Zhongkai Hao, Zhengyi Wang, Hang Su, Chengyang Ying, Yinpeng Dong, Songming Liu, Ze Cheng, Jian Song, and Jun Zhu. Gnot: A general neural operator transformer for operator learning. In International Conference on Machine Learning, pages 12556–12569. PMLR, 2023.
- Irina Higgins, Loic Matthey, Arka Pal, Christopher Burgess, Xavier Glorot, Matthew Botvinick, Shakir Mohamed, and Alexander Lerchner. beta-VAE: Learning basic visual concepts with a constrained variational framework. In International Conference on Learning Representations, 2022.
- Jonathan Ho, Ajay Jain, and Pieter Abbeel. Denoising diffusion probabilistic models. Advances in Neural Information Processing Systems, 33:6840–6851, 2020.
- Marc C Kennedy and Anthony O’Hagan. Predicting the output from a complex computer code when fast approximations are available. Biometrika, 87(1):1–13, 2000.
- Gavin Kerrigan, Giosue Migliorini, and Padhraic Smyth. Functional flow matching. In International Conference on Artificial Intelligence and Statistics, pages 3934–3942. PMLR, 2024.
- Diederik P Kingma and Max Welling. Auto-encoding variational bayes. arXiv preprint arXiv:1312.6114, 2013.
- Leon Klein, Andreas Krämer, and Frank Noé. Equivariant flow matching. Advances in Neural Information Processing Systems, 36, 2023.
- Tamara Gibson Kolda. Multilinear operators for higher-order decompositions, volume 2. United States. Department of Energy, 2006.
- Zhifeng Kong and Wei Ping. On fast sampling of diffusion probabilistic models. In ICML Workshop on Invertible Neural Networks, Normalizing Flows, and Explicit Likelihood Models, 2021.
- Nikola B Kovachki, Zongyi Li, Burigede Liu, Kamyar Aizzadenesheli, Kaushik Bhattacharya, Andrew M Stuart, and Anima Anandkumar. Neural operator: Learning maps between function spaces with applications to pdes. J. Mach. Learn. Res., 24(89):1–97, 2023.

- Hugo Larochelle and Iain Murray. The neural autoregressive distribution estimator. In Proceedings of the fourteenth international conference on artificial intelligence and statistics, pages 29–37. JMLR Workshop and Conference Proceedings, 2011.
- Yann LeCun, Sumit Chopra, Raia Hadsell, M Ranzato, and Fugie Huang. A tutorial on energy-based learning. Predicting structured data, 1(0), 2006.
- Shibo Li, Zheng Wang, Robert M Kirby, and Shandian Zhe. Deep multi-fidelity active learning of high-dimensional outputs. Proceedings of the Twenty-Fifth International Conference on Artificial Intelligence and Statistics, 2022a.
- Zijie Li, Kazem Meidani, and Amir Barati Farimani. Transformer for partial differential equations’ operator learning. arXiv preprint arXiv:2205.13671, 2022b.
- Zongyi Li, Nikola Kovachki, Kamyar Azizzadenesheli, Burigede Liu, Kaushik Bhattacharya, Andrew Stuart, and Anima Anandkumar. Neural operator: Graph kernel network for partial differential equations. arXiv preprint arXiv:2003.03485, 2020a.
- Zongyi Li, Nikola Borislavov Kovachki, Kamyar Azizzadenesheli, Kaushik Bhattacharya, Andrew Stuart, Anima Anandkumar, et al. Fourier neural operator for parametric partial differential equations. In International Conference on Learning Representations, 2020b.
- Yaron Lipman, Ricky TQ Chen, Heli Ben-Hamu, Maximilian Nickel, and Matt Le. Flow matching for generative modeling. arXiv preprint arXiv:2210.02747, 2022.
- Da Long, Nicole Mrvaljevic, Shandian Zhe, and Bamdad Hosseini. A kernel approach for pde discovery and operator learning. arXiv preprint arXiv:2210.08140, 2022.
- Lu Lu, Pengzhan Jin, Guofei Pang, Zhongqiang Zhang, and George Em Karniadakis. Learning nonlinear operators via deeponet based on the universal approximation theorem of operators. Nature machine intelligence, 3(3):218–229, 2021.
- Lu Lu, Xuhui Meng, Shengze Cai, Zhiping Mao, Somdatta Goswami, Zhongqiang Zhang, and George Em Karniadakis. A comprehensive and fair comparison of two neural operators (with practical extensions) based on fair data. Computer Methods in Applied Mechanics and Engineering, 393:114778, 2022.
- Andrew Ronald Mitchell and David Francis Griffiths. The finite difference method in partial differential equations. Number BOOK. John Wiley, 1980.
- Shakir Mohamed and Balaji Lakshminarayanan. Learning in implicit generative models. arXiv preprint arXiv:1610.03483, 2016.
- George Papamakarios, Theo Pavlakou, and Iain Murray. Masked autoregressive flow for density estimation. Advances in neural information processing systems, 30, 2017.
- Carl Edward Rasmussen and Christopher K. I. Williams. Gaussian Processes for Machine Learning. MIT Press, 2006.
- Saman Razavi, Bryan A Tolson, and Donald H Burn. Review of surrogate modeling in water resources. Water Resources Research, 48(7), 2012.
- Danilo Jimenez Rezende, Shakir Mohamed, and Daan Wierstra. Stochastic backpropagation and approximate inference in deep generative models. In International conference on machine learning, pages 1278–1286. PMLR, 2014.

- Robin Rombach, Andreas Blattmann, Dominik Lorenz, Patrick Esser, and Björn Ommer. High-resolution image synthesis with latent diffusion models. In Proceedings of the IEEE/CVF conference on computer vision and pattern recognition, pages 10684–10695, 2022.
- Tim Salimans and Jonathan Ho. Progressive distillation for fast sampling of diffusion models. arXiv preprint arXiv:2202.00512, 2022.
- Tim Salimans, Ian Goodfellow, Wojciech Zaremba, Vicki Cheung, Alec Radford, and Xi Chen. Improved techniques for training gans. Advances in neural information processing systems, 29, 2016.
- Andy Shih, Suneel Belkhale, Stefano Ermon, Dorsa Sadigh, and Nima Anari. Parallel sampling of diffusion models. Advances in Neural Information Processing Systems, 36, 2023.
- Jiaming Song, Chenlin Meng, and Stefano Ermon. Denoising diffusion implicit models. In International Conference on Learning Representations, 2021a.
- Yang Song and Diederik P Kingma. How to train your energy-based models. arXiv preprint arXiv:2101.03288, 2021.
- Yang Song, Jascha Sohl-Dickstein, Diederik P Kingma, Abhishek Kumar, Stefano Ermon, and Ben Poole. Score-based generative modeling through stochastic differential equations. In International Conference on Learning Representations, 2021b. URL <https://openreview.net/forum?id=PXTIG12RRHS>.
- Sibo Tian, Minghui Zheng, and Xiao Liang. Transfusion: A practical and effective transformer-based diffusion model for 3d human motion prediction. IEEE Robotics and Automation Letters, 2024.
- Aäron Van Den Oord, Nal Kalchbrenner, and Koray Kavukcuoglu. Pixel recurrent neural networks. In International conference on machine learning, pages 1747–1756. PMLR, 2016.
- Martin J Wainwright, Michael I Jordan, et al. Graphical models, exponential families, and variational inference. Foundations and Trends® in Machine Learning, 1(1–2):1–305, 2008.
- Ye Yuan and Kris Kitani. Dlow: Diversifying latent flows for diverse human motion prediction. In Computer Vision–ECCV 2020: 16th European Conference, Glasgow, UK, August 23–28, 2020, Proceedings, Part IX 16, pages 346–364. Springer, 2020.
- Biao Zhang and Peter Wonka. Functional diffusion. In Proceedings of the IEEE/CVF Conference on Computer Vision and Pattern Recognition, pages 4723–4732, 2024.
- Qinsheng Zhang and Yongxin Chen. Fast sampling of diffusion models with exponential integrator. In The Eleventh International Conference on Learning Representations, 2023.
- Olgierd Cecil Zienkiewicz, Robert Leroy Taylor, Olgierd Cecil Zienkiewicz, and Robert Lee Taylor. The finite element method, volume 36. McGraw-hill London, 1977.

Appendix

Appendix A. Mult-Physics Systems Details

A.1 Darcy Flow

We considered a single-phase 2D Darcy flow system, which is governed by the following PDE,

$$\begin{aligned} -\nabla \cdot (a(\mathbf{x})\nabla u(\mathbf{x})) &= f(\mathbf{x}) \quad \mathbf{x} \in (0, 1)^2 \\ u(\mathbf{x}) &= 0, \quad \mathbf{x} \in \partial(0, 1)^2, \end{aligned} \quad (14)$$

where $a(\mathbf{x})$ is the permeability field, $u(\mathbf{x})$ is the fluid pressure, and $f(\mathbf{x})$ is the external source, representing sources or sinks of the fluid. To obtain one instance of the triplet (a, f, u) , we sampled f from a Gauss random field: $f \sim \mathcal{N}(0, (-\Delta + 25)^{-\frac{15}{2}})$, and a from the exponential of a Gaussian random field: $a = \exp(g)$ where $g \sim \mathcal{N}(0, (-\Delta + 16)^{-2})$. We then ran a second-order finite-difference solver to obtain u at a 256×256 mesh. To prepare irregularly-sampled data, we randomly selected 1,200 to 1,500 input locations and their corresponding function values from the mesh. To prepare regularly-sampled data, we extracted each function instance from a 64×64 sub-mesh.

A.2 Convection Diffusion

We considered a 1D convection-diffusion system, governed by the following PDE,

$$\frac{\partial u(x, t)}{\partial t} + \nabla \cdot (v(x, t)u(x, t)) = D\nabla^2 u(x, t) + s(x, t), \quad (15)$$

where $(x, t) \in [-1, 1] \times [0, 1]$, $u(x, 0) = 0$, D is the diffusion coefficient and was set to 0.01, $v(x, t)$ is the convection velocity, describing how fast the substance is transported due to the flow, $s(x, t)$ is the source term, representing the external force, and $u(x, t)$ is the quantity of interest, such as the temperature, concentration and density. We employed a parametric form for v and a : $v(x, t) = \sum_{n=1}^3 a_n x^n + a_4 t$, and $s(x, t) = \alpha \exp(-\beta(x+t)^2) + \gamma \cos(\eta \cdot \pi(x-0.1t))$, where all $a_n, \alpha, \beta, \gamma, \eta$ are sampled from $\text{Uniform}(-1, 1)$. We used the MATLAB PDE solver `pdepe`¹ to obtain the solution for u . The spatial-temporal domain was discretized into a 512×256 mesh. To prepare irregularly-sampled data, we randomly selected 1,200 to 1,500 input locations and their corresponding function values from the mesh. To prepare regularly-sampled data, we extracted each function instance from a 64×64 sub-mesh.

A.3 Torus Fluid

We considered a viscous, incompressible fluid on the unit torus. The governing equation in vorticity form is given by

$$\frac{\partial w(\mathbf{x}, t)}{\partial t} + \mathbf{u} \cdot \nabla w(\mathbf{x}, t) = \nu \nabla^2 w(\mathbf{x}, t) + f(\mathbf{x}), \quad (16)$$

$$w(\mathbf{x}, 0) = w_0(\mathbf{x}), \quad (17)$$

where $\mathbf{x} \in [0, 1]^2$, $t \in [0, 10]$, $\nu = 0.001$, \mathbf{u} is the velocity field that $\nabla \cdot \mathbf{u} = 0$, $w(\mathbf{x}, t)$ is the vorticity function, and $f(\mathbf{x})$ is the source function that represents the external forces. We are interested in seven spatial functions: the initial condition w_0 , the source function f , and the vorticity fields at time steps $t = 2, 4, 6, 8, 10$, denoted as w_1, w_2, w_3, w_4 , and w_5 . We employed a parametric form for w_0 and f : $w_0(\mathbf{x}) = [\sin(\alpha_1 \pi(x_1 + \beta_1)), \sin(\alpha_2 \pi(x_1 + \beta_2))] \cdot \mathbf{\Lambda} \cdot [\cos(\alpha_1 \pi(x_2 + \beta_1)), \cos(\alpha_2 \pi(x_2 + \beta_2))]^T$, where $\alpha_1, \alpha_2 \sim \text{Uniform}(0.5, 1)$, $\beta_1, \beta_2 \sim \text{Uniform}(0, 1)$, and each $[\mathbf{\Lambda}]_{ij} \sim \text{Uniform}(-1, 1)$, and $f(x_1, x_2) = 0.1 (a \sin(2\pi(x_1 + x_2 + c)) + b \cos(2\pi(x_1 + x_2 + d)))$ where $a, b \sim \text{Uniform}(0, 2)$ and $c, d \sim \text{Uniform}(0, 0.5)$.

1. <https://www.mathworks.com/help/matlab/math/partial-differential-equations.html>

We used the finite-difference solver as provided in (Li et al., 2020b) to obtain the solution of $\{w_1, w_2, w_3, w_4, w_5\}$. The spatial domain was discretized to a 128×128 mesh. Again, to prepare the irregularly-sampled training and test data, we randomly selected 1,200 to 1,500 locations and the corresponding function values from the mesh. To prepare the regularly-sampled data, we extracted the function instances from a 64×64 sub-mesh.

Appendix B. Hyperparameter Selection

In the experiment, we used the validation dataset to determine the optimal hyperparameters for each method. The set of the hyperparameters and their respective ranges are listed as follows.

- FNO: the hyperparameters include the number of modes, which varies from $\{12, 16, 18, 20, 24\}$, the number of channels for channel lifting, which varies from $\{64, 128, 256\}$, and the number of Fourier layers, which varies from $\{2, 3, 4, 5\}$. We used GELU activation, the default choice in the original FNO library².
- DON: the hyperparameters include the number of convolution layers in the branch net, which varies from $\{3, 5, 7\}$, the kernel size in the convolution layer, which varies from $\{3, 5, 7\}$, the number of MLP layers in the trunk net, which varies from $\{3, 4, 5\}$, the output dimension of the branch net and trunk net, which varies from $\{64, 128, 256\}$, and the activation, which varies from $\{\text{ReLU}, \text{Tanh}\}$.
- PODDON: the hyperparameters include the number of bases, varying from $\{128, 256, 512\}$, the number of convolution layers in the branch net, varying from $\{3, 5, 7\}$, the kernel size, varying from $\{3, 5, 7\}$, the output dimension of the branch net and trunk net, varying from $\{64, 128, 256\}$, and the activation, varying from $\{\text{ReLU}, \text{Tanh}\}$.
- GNOT: the hyperparameters include the number of attention layers, varying from $\{3, 4, 5\}$, the dimensions of the embeddings, varying from $\{64, 128, 256\}$, and the inclusion of mixture-of-expert-based gating, specified as either $\{\text{yes}, \text{no}\}$. We used GELU activation, the default choice of the original library³.
- ACM-FD: the hyperparameters include the number of modes, which varies from $\{12, 16, 18, 20, 24\}$, the number of channels for channel lifting, which varies from $\{64, 128, 256\}$, the number of Fourier layers from, which varies from $\{3, 4, 5\}$, the length-scale of the SE kernel, which varies from $\{1e-2, 5e-3, 1e-3, 5e-4, 1e-4\}$. We used GELU activation.
- β -VAE: the hyperparameters include β , varying from $\{1e1, 1e-1, 1e-3, 1e-4, 1e-5, 1e-6\}$, the rank, varying from $\{16, 32, 64, 128, 256\}$, and the number of convolution layers in the decoder and encoder networks, varying from $\{1, 2, 3, 4\}$. We employed the GELU activation and fixed the kernel size to be 3.

For each competing method, each task underwent a separate hyperparameter tuning process to identify the optimal hyperparameters specific to that task. In contrast, for ACM-FD, we tuned the model only once, where the validation error is defined as the summation of the relative L_2 error across all tasks. The tuning of β -VAE is guided by the reconstruction error on the validation dataset.

2. <https://github.com/neuraloperator/neuraloperator>

3. <https://github.com/HaoZhongkai/GNOT>

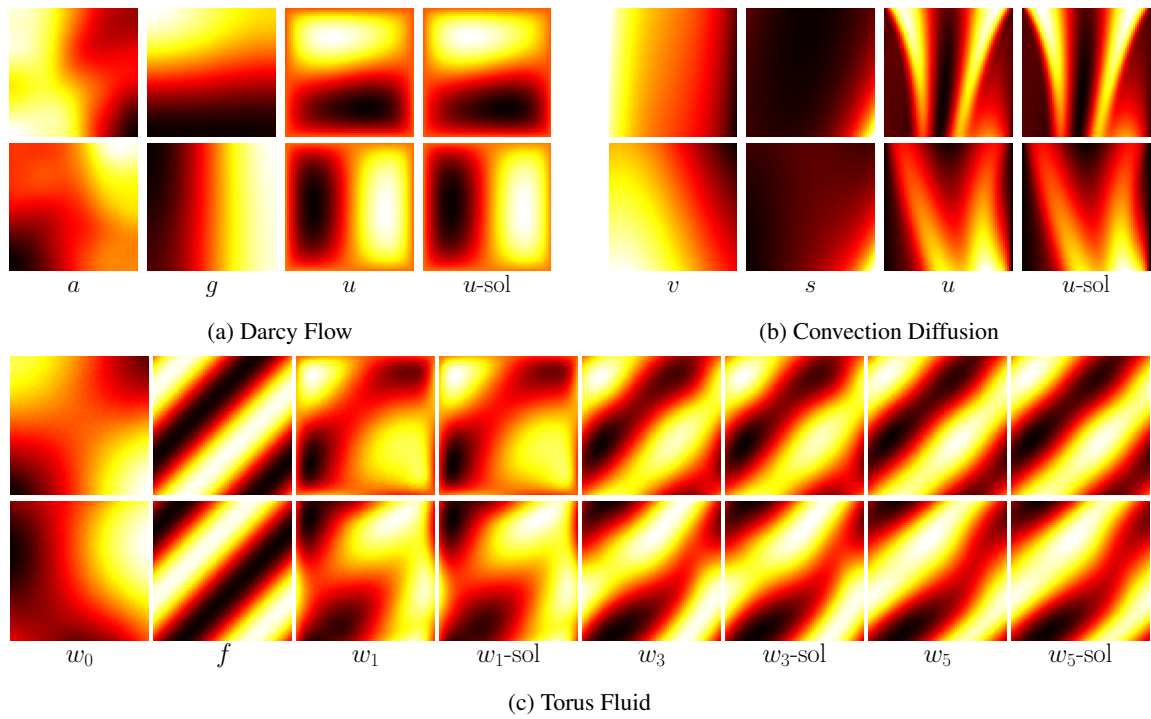


Figure 2: More Generated Function Instances By ACM-FD. "-sol" Means The Numerical Solution Provided By The Numerical Solvers Given The Other Functions.